JBC RESEARCH ARTICLE

Rab5 nucleotide binding promotes oxidative metabolism to fuel hepatocellular carcinoma cell proliferation

Received for publication, December 5, 2025, and in revised form, February 13, 2026 Published, Papers in Press, February 25, 2026
https://doi.org/10.1016/j.jbc.2026.111321

Kelly O. Otakhor[1], Mohd Ali Abbas Zaidi[2], Rebecca E. Oberley-Deegan[2], Moorthy P. Ponnusamy[2], Kurt W. Fisher[3], and Micah B. Schott[2,*]

From the [1]Department of Genetics, Cell Biology and Anatomy, University of Nebraska Medical Center, Omaha, Nebraska, USA; [2]Department of Biochemistry and Molecular Biology, University of Nebraska Medical Center, Omaha, Nebraska, USA; and [3]Department of Pathology, Microbiology and Immunology, University of Nebraska Medical Center, Omaha, Nebraska, USA

Reviewed by members of the JBC Editorial Board. Edited by Qi-Qun Tang

Altered lipid metabolism and lipid droplet (LD) dynamics are features of certain hepatocellular carcinoma (HCC) subtypes, but the molecular mechanisms governing LD trafficking and catabolism in HCC cells remain unclear. The small GTPase Rab5, a key regulator of early endosomal dynamics, has been previously observed to localize to the surface of LDs and participate in LD degradation through microlipophagy. However, the regulation of Rab5–LD interactions and its functional consequences in HCC cell metabolism and proliferation have not been elucidated. In this study, we explored the role of Rab5 in governing LD homeostasis and its impact on HCC cell proliferation. We found that GTP-bound Rab5 mutants (Q79L) exhibited increased association with LDs compared with the GDP-bound mutants (S34N) and WT Rab5. Acute nutrient starvation enhanced Rab5 GTP loading and recruitment to LDs, indicating that Rab5's GTPase cycle regulates its LD localization. Importantly, inhibition of Rab5 GTP binding led to increased LD accumulation, reduced mitochondrial respiration, and impaired proliferation in HCC cell lines. Transcriptomic analyses and tissue microarray immunohistochemistry further revealed that Rab5 is significantly overexpressed in HCC patient samples. These findings suggest that Rab5 GTP binding is an important contributor to LD dynamics in HCC cells, helping to govern LD turnover to sustain mitochondrial energy production and support cancer cell proliferation.

Hepatocellular carcinoma (HCC) is currently the fourth leading cause of cancer-related deaths worldwide, characterized by a poor 5-year survival rate largely because of its aggressive clinical course and limited effective treatment options (1–4). While several targeted therapies have emerged, therapeutic resistance and high recurrence rates continue to challenge long-term disease management (1, 3). In recent years, the global prevalence of obesity and excessive alcohol intake has significantly contributed to the surge in HCC incidence (5–8). As a result, both metabolic dysfunction–associated steatotic liver disease and metabolic dysfunction–associated steatohepatitis are rapidly becoming the predominant underlying causes of liver cancer, even in the absence of viral hepatitis (9, 10). Despite the well-established link between steatotic liver disease and HCC development (11), the role of excess lipids in promoting tumor progression remains underexplored.

Excess lipids are stored within specialized organelles known as lipid droplets (LDs), which store neutral lipids, such as triacylglycerol and cholesteryl ester, within the cytoplasm. Catabolism of LDs leads to fatty acid release, providing lipid substrates that support energy homeostasis in a subset of HCC tumors (12). A major driver of LD catabolism is lipophagy, the selective autophagic degradation of LDs within lysosomes. Lipophagy can occur through two main routes: macrolipophagy, whereby entire LDs are enclosed within double-membrane autophagosomes, and microlipophagy, whereby LDs are directly engulfed by endolysosomes without the formation of a classical autophagosome (13, 14). The latter form of LD degradation is evolutionarily conserved from yeast to mammals and has been documented in multiple mammalian cell types, including hepatocytes and macrophages (15–20). Within the acidic lysosome, lysosomal acid lipase hydrolyzes neutral lipids, liberating free fatty acids that can be directed toward mitochondrial β-oxidation or utilized as building blocks for membrane biosynthesis (11, 21). While the enzymatic steps of lipid degradation are well characterized, the upstream processes that govern LD recognition, intracellular trafficking, and lysosomal targeting remain poorly defined. Emerging evidence indicates that cancer cells exploit lipophagy to sustain energy homeostasis and support unchecked proliferation (21, 22). However, in the context of HCC, the molecular regulators orchestrating LD mobilization through this pathway are still largely unknown, highlighting a critical gap in our understanding of tumor metabolism.

Multiple proteomic analyses of LDs have identified a variety of Rab GTPases enriched on the LD surface (23–27). While Rab proteins are broadly recognized as key regulators of intracellular vesicle trafficking (28), the specific roles of many Rab family members in LD dynamics remain largely unexplored. Among them, Rab5 stands out for its well-established function in early endosomal trafficking and

* For correspondence: Micah B. Schott, mschott@unmc.edu.

© 2026 THE AUTHORS. Published by Elsevier Inc on behalf of American Society for Biochemistry and Molecular Biology. This is an open access article under the CC BY license (http://creativecommons.org/licenses/by/4.0/).

membrane transport (29–31). Its activity is tightly regulated through a cycle of GDP- (inactive) and GTP-bound (active) states, coordinated by guanine nucleotide exchange factors, GTPase-activating proteins (GAPs), and GDP dissociation inhibitors (31, 32). Once activated, GTP-bound Rab5 recruits its effector proteins, such as early endosome antigen 1 (EEA1), orchestrating the spatial and temporal control of membrane trafficking events (33). While traditionally studied in the context of endocytosis (34, 35), emerging evidence suggests that Rab5 has broader roles in organelle communication and autophagy (36–40). Notably, Rab5 has been observed on the surface of LDs (36). Our recent work has shown that Rab5 localizes to LDs and participates in LD trafficking to lysosomes, implicating it as an important regulator of microlipophagy (13). However, how Rab5 is recruited to LDs, how its GTP–GDP binding activity modulates this process, and whether it plays a direct role in LD turnover in HCC remain open questions.

In this study, we integrate super-resolution microscopy, biochemical assays, and Seahorse metabolic analysis to further explore the role of Rab5 in coordinating LD catabolism and metabolic adaptation in HCC. We show that under nutrient-limited conditions where lipophagy is active, Rab5 also undergoes activation into its GTP-bound form and is preferentially recruited to LDs. Inhibition of Rab5 GTP binding leads to LD accumulation and a reduction in mitochondrial respiration, thereby reducing HCC cell proliferation and spheroid growth.

Results

Rab5 is recruited to LDs in a GTPase-dependent manner in HCC cells

How Rab5 GTP–GDP binding activity mediates LD recruitment has not been fully elucidated, particularly in HCC. To assess this, Hep3B human hepatoma cells were transfected with either WT GFP-Rab5A, a constitutively active GTP-bound mutant (GFP-Rab5A Q79L), or a dominant-negative GDP-bound mutant (GFP-Rab5A S34N). We then analyzed the localization of these Rab5 variants relative to LDs stained with Oil Red O (ORO) using super-resolution confocal microscopy. As shown in Figure 1*A*,

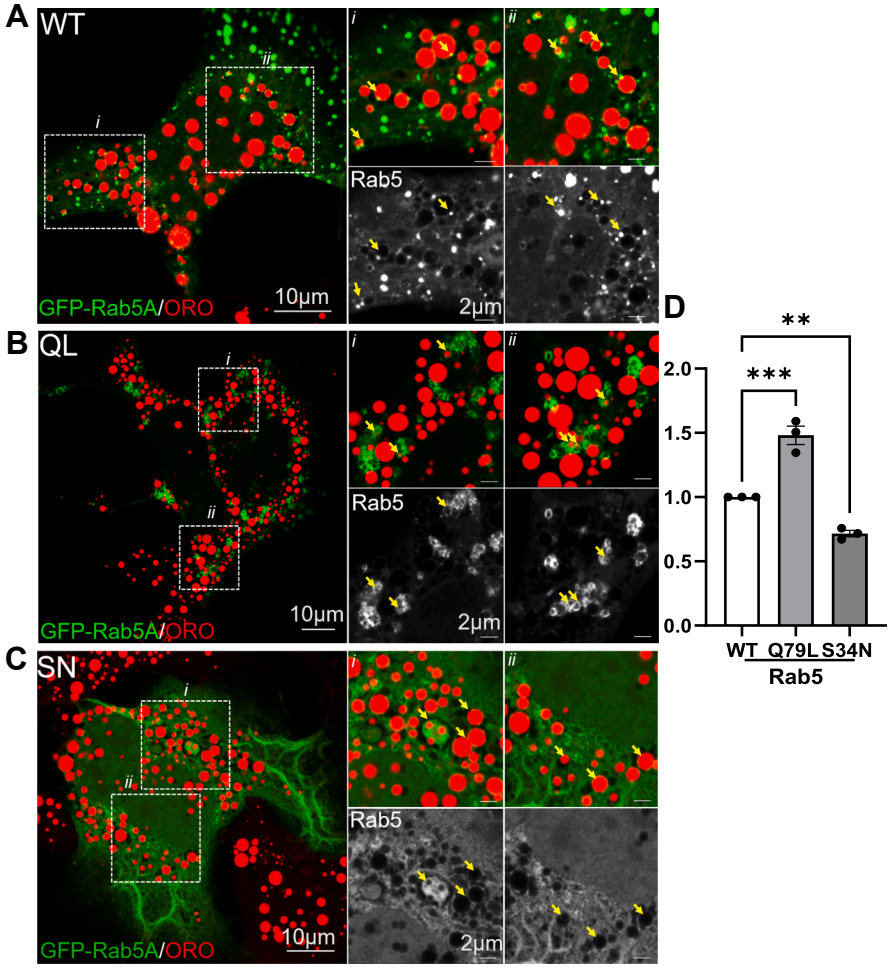


Figure 1. Rab5 is recruited to lipid droplets (LDs) in a GTPase-dependent manner in Hep3B cells. Super-resolution confocal micrographs of Hep3B human hepatoma cells expressing (*A*) WT Rab5 (GFP-Rab5 WT), (*B*) constitutively active mutant (GFP-Rab5 Q79L), and (*C*) dominant-negative mutant (GFP-Rab5 S34N). LDs were stained with Oil Red O (ORO, *red*) to visualize neutral lipid stores. GFP-Rab5 fluorescence (*green*) marks Rab5 localization. Inlays depict Rab5 localization around LD borders, indicated further by *yellow arrows*. *D*, quantification of Rab5–LD colocalization by the ratio of LD:cytoplasm GFP-Rab5 intensity. Graphs represent mean ± SD from n = 3 independent experiments. Statistical significance was determined using one-way ANOVA with Tukey's post hoc test. $^{**}p < 0.01$ and $^{***}p < 0.001$.

cells expressing WT GFP-Rab5 display moderate localization of Rab5 puncta adjacent to ORO-labeled LDs (*yellow arrows*). Notably, expression of "active" GFP-Rab5 Q79L (Fig. 1*B*) resulted in markedly enhanced localization of Rab5 to LDs. This was evident as robust GFP-Rab5 puncta outlined and fully engulfed the LDs. Interestingly, GFP-Rab5 Q79L appeared to preferentially associate with smaller LDs, consistent with previous work showing that smaller LDs are more amenable to lipophagy (41). Also, the GFP-Rab5(Q79L) vesicles formed enlarged, highly fused endosomal structures engulfing smaller LDs. Cells expressing the GDP-bound inactive GFP-Rab5 S34N mutant (Fig. 1*C*) also exhibited interaction around LDs, although there was much more prominent cytoplasmic localization compared with WT and QL Rab5. Quantification of Rab5 localization to LDs was calculated by measuring the ratio of LD-adjacent *versus* cytoplasmic GFP intensity ratios, which revealed a ∼1.7-fold greater localization of Rab5 Q79L association with LDs relative to Rab5 WT, whereas Rab5 S34N displayed a reduced LD localization compared with Q79L (Fig. 1*D*). These data suggest that the GTP-bound active form of Rab5 localizes more exclusively to LDs in Hep3B cells, whereas the GDP-bound Rab5 also localizes but to a lesser degree, suggesting that Rab5–LD interaction is regulated by Rab5's nucleotide binding state.

Enhanced recruitment of Rab5 to LDs during nutrient starvation

Next, as nutrient deprivation is known to stimulate lipophagy (18, 42, 43), we evaluated the effect of Hank's balanced salt solution (HBSS) starvation on Rab5–LD recruitment as well as Rab5 GTP–GDP binding. Hep3B cells were starved for 4 h in HBSS, and GTP-bound Rab5 levels were assessed by pull-down with GTP–agarose beads. As shown in Figure 2, *A* and *B*, HBSS starvation resulted in a >50% increase in Rab5 GTP–binding activity compared with cells maintained in complete medium (CM; control). Levels of the Rab5-interacting protein EEA1 did not change significantly between starved and control cells (Fig. 2, *A* and *B*), and total Rab5 levels did not change between control and HBSS-treated cells (Fig. 2*C*). To confirm that GTP pulldown was specific for

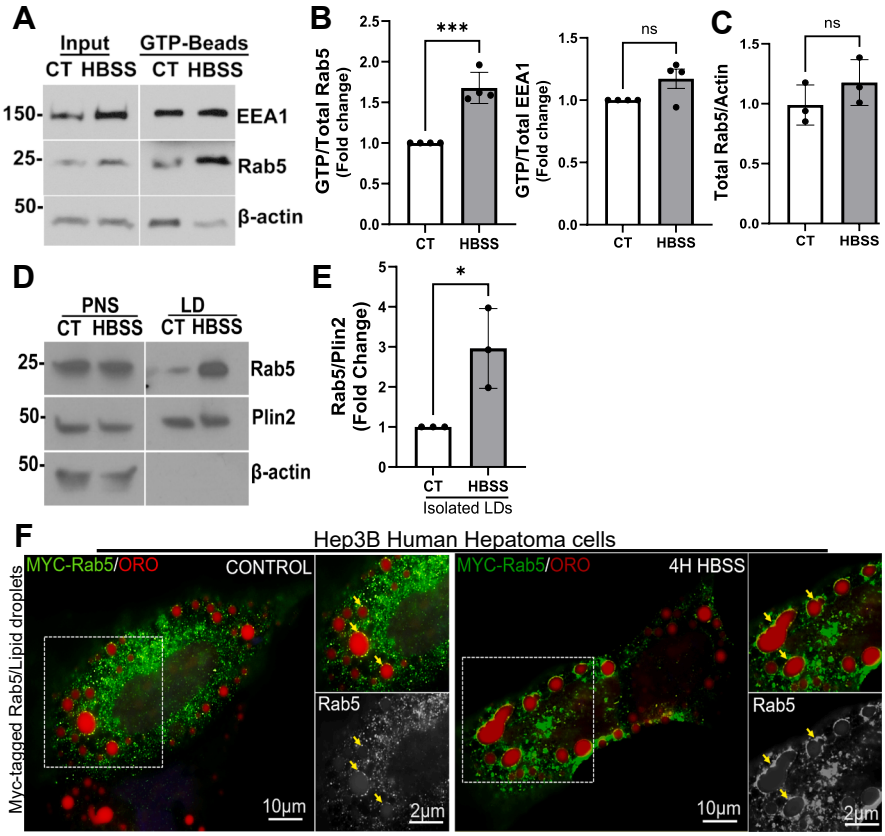


Figure 2. Enhanced recruitment of Rab5 to lipid droplets (LDs) upon lipophagy stimulation. *A*, Western blot analysis of Rab5 and EEA1 GTP-pulldown in regular medium (CT) or 4 h HBSS starvation in Hep3B cells. *B*, quantification of the fold change of GTP-bound/total Rab5 as well as EEA1 from n = 4 independent experiments. *C*, quantification of total Rab5–β-actin confirming that starvation does not change overall Rab5 expression. *D*, Western blot analysis of LDs isolated from Hep3B cells by density gradient centrifugation showing abundant levels of Rab5 in isolated LDs following 4 h of HBSS starvation compared with the regular medium (CT). *E*, quantification of Rab5–Plin2 in the biochemically isolated LDs. *F*, fluorescence micrograph showing immunofluorescence staining of Hep3B cells expressing Myc-tagged Rab5 (*green*). Cells were treated with oleic acid for 16 h and then either maintained in regular medium (control) or subjected to 4 h of HBSS starvation before being fixed and stained with Oil Red O (ORO; *red*) to label LDs. Note the marked increase in Rab5 staining around LDs in HBSS-starved cells *versus* control (*yellow arrowheads*). Graphs represent mean ± SD from n = 3 to 4 independent experiments. Statistical significance was determined using an unpaired two-tailed *t* test. *$p < 0.05$, **$p < 0.01$, and ***$p < 0.001$. CT, control; EEA1, early endosome antigen 1; HBSS, Hank's balanced salt solution; Plin2, perilipin-2.

active, GTP-bound Rab5, we further validated this assay by robust pulldown of GTP-locked Myc-Rab5 Q79L but not the GDP-bound Myc-Rab5 S34N mutant (Fig. S1*A*). Together, these findings are consistent with results from Figure 1*A*, as well as previous reports showing Rab5 enrichment in LD fractions treated with a nonhydrolyzable GTP analog (GTPγS) (36).

Given our findings that HBSS increased Rab5 GTP binding and that constitutively active GFP-Rab5(Q79L) mutants exhibit greater association with LDs, we sought to determine the effect of HBSS starvation on endogenous Rab5 recruitment to LDs. Hep3B cells were first loaded with oleic acid (OA; 150 μM, 16 h) to induce LD formation, then the cells were starved for 4 h in HBSS. LDs were then isolated by density gradient centrifugation, and Rab5 was assessed by Western blot analysis. As shown in Figure 2, *D* and *E*, Rab5 levels were elevated two- to fourfold in LD fractions in starved cells compared with control cells maintained in CM, indicating enhanced recruitment of Rab5 to LDs under conditions that promote lipophagy activation. Perilipin-2 (PLIN-2) served as an LD marker and loading control, whereas the absence of β-actin in LD fractions confirms the lack of cytoplasmic contaminants. Consistent with enhanced LD catabolism, HBSS starvation significantly reduced LD number and total LD area per cell in both basal and OA-loaded Hep3B cells (Fig. S2, *B–E*), indicating that acute HBSS starvation decreases LD abundance. This finding was further corroborated by immunofluorescence microscopy of Hep3B cells expressing Myc-tagged Rab5A (*green*), which exhibited a predominantly punctate cytoplasmic distribution with limited localization with ORO-stained LDs (*red*) in cells maintained in control medium. However, Myc-Rab5A was more predominantly localized around LDs following HBSS-induced starvation, as indicated by *white arrows*. This enhanced localization suggests increased Rab5 recruitment to LDs under nutrient-deprived conditions, consistent with its role in mediating microlipophagy (13). These results indicate that Rab5 is not only recruited to LDs during nutrient deprivation but also activated through GTP loading.

The pharmacological inhibition of Rab5 activity decreases LD catabolism and GTPase activity

Building on our findings that nutrient starvation activates Rab5 and increases its recruitment to LDs, we next sought to determine the impact of Rab5 GTP–binding activity on LD catabolism. To test this, we utilized the small molecule neoandrographolide (NAP), which has been previously identified as a selective inhibitor of Rab5 GTPase activity (44). We first validated the effect of NAP on Rab5-GTP binding using GTP–agarose beads in Hep3B cells. As expected, treatment with NAP (100 μM, 48 h) resulted in a >90% reduction in Rab5 activity (Fig. 3, *A* and *B*). Furthermore, NAP treatment resulted in a marked increase in both LD number and total

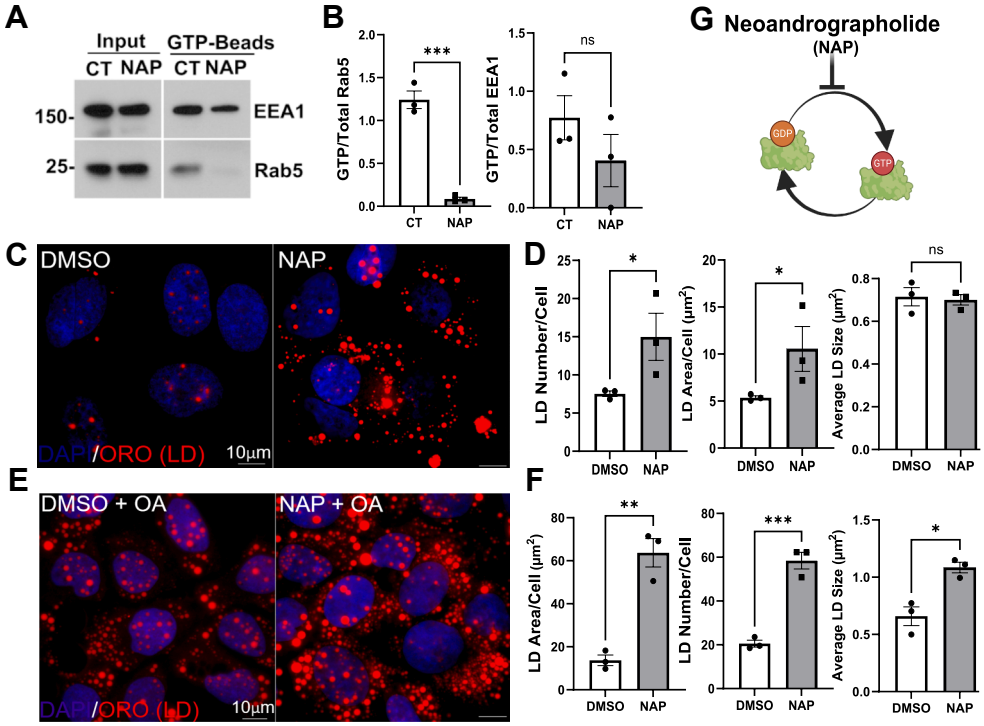


Figure 3. Inhibition of Rab5 GTPase activity reduces lipid droplet (LD) catabolism *via* its GTPase activity. *A*, Western blot analysis of Rab5 and EEA1 GTP-pulldown in Hep3B cells treated with DMSO (CT) or NAP (100 μM, 48 h). *B*, quantification of GTP/total Rab5 as well as EEA1 from n = 3 independent experiments. *C*, confocal micrograph showing ORO-stained LDs (*red*) and DAPI-stained nuclei from Hep3B cells treated with DMSO (control) and NAP (100 μM). *D*, bar graphs depict quantification of LD number/cell, total LD area/cell, and LD size. *E*, confocal micrograph showing ORO-stained LDs (*red*) and DAPI-stained nucleus from Hep3B cells treated with DMSO (control) and NAP (100 μM) with oleic acid (OA, 150 μM). *F*, bar graphs depict quantification of LD number/cell, total LD area/cell, and LD size. *G*, *cartoon* depicting NAP alteration of Rab5 GTP binding. *Graphs* represent mean ± SD from n = 3 independent experiments. Statistical significance was determined using an unpaired two-tailed *t* test. *$p < 0.05$, **$p < 0.01$, and ***$p < 0.001$. CT, control; DAPI, 4′,6-diamidino-2-phenylindole; DMSO, dimethyl sulfoxide; EEA1, early endosome antigen 1; NAP, neoandrographolide; ORO, Oil Red O.

area per cell, compared with dimethyl sulfoxide (DMSO)–treated controls (Fig. 3*C*). Quantitative analysis (Fig. 3*D*) demonstrated an approximately two- to threefold increase in total LD area per cell upon Rab5 inhibition, with no significant change in average LD size, but an approximately threefold increase in LD number per cell. The effect of NAP was especially visible in Hep3B cells loaded with OA (150 μM, 16 h), as shown in Figure 3, *E* and *F*, where we observed an approximately fivefold increase in LD area per cell, an approximately 1.5-fold increase in LD size, and an approximately threefold increase in LD number per cell following Rab5 inhibition. To test whether the effect of Rab5 inhibition on LDs extends beyond HCC cell lines, we also performed ORO staining in breast cancer (MDA-MB-231) and pancreatic cancer (KPC8060) cell lines treated with NAP. In both cell types, NAP caused a clear accumulation of LDs, indicating that NAP-sensitive suppression of LD catabolism is observed across multiple cancer cell types (Fig. S4, *A*–*D*). These results collectively indicate that Rab5 GTP–binding activity is an important contributor to LD catabolism in cancer cells.

Inhibition of Rab5 GTP–GDP binding activity impairs mitochondrial respiration in HCC cells

To test the impact of Rab5 GTP binding on mitochondrial respiration, we performed Seahorse metabolic analysis in DMSO *versus* NAP-treated Hep3B cells to measure oxygen consumption rate (OCR), basal respiration, and spare respiratory capacity. We focused on spare respiratory capacity as a marker of mitochondrial fitness and metabolic flexibility, reflecting the ability of mitochondria to increase ATP production in response to increased energy demand (45, 46). As shown in Figure 4, Rab5 inhibition significantly suppressed OCR in both CM and upon nutrient deprivation (HBSS, 4 h). In CM (Fig. 4, *A* and *B*), NAP-treated cells showed a pronounced reduction in both basal respiration and spare respiratory capacity, indicating a loss of mitochondrial responsiveness and energy-generating potential. Under 4 h of HBSS starvation (Fig. 4, *C* and *D*), Rab5 inhibition continued to suppress OCR, further reducing both basal and spare capacity, suggesting that Rab5 is critical for sustaining mitochondrial oxidative metabolism, especially under conditions that promote lipophagy stimulation. Notably, HBSS alone was sufficient to maintain near-baseline mitochondrial respiration while limiting spare capacity (Fig. S2*A*). Taken together, these data indicate that Rab5 inhibition impairs mitochondrial respiration in HCC cells.

Inhibition of Rab5 GTP–GDP binding activity decreases HCC cell proliferation

To investigate the functional consequences of Rab5 GTP–GDP–binding activity inhibition on tumorigenic potential, we assessed the ability of HCC cells to form colonies and spheroids upon disruption of Rab5 activity. HCC cell lines (Hep3B and Huh7) were subjected to colony formation and 3D spheroid assays following treatment with NAP. In the colony formation assay (Fig. 5*A*), untreated control cells

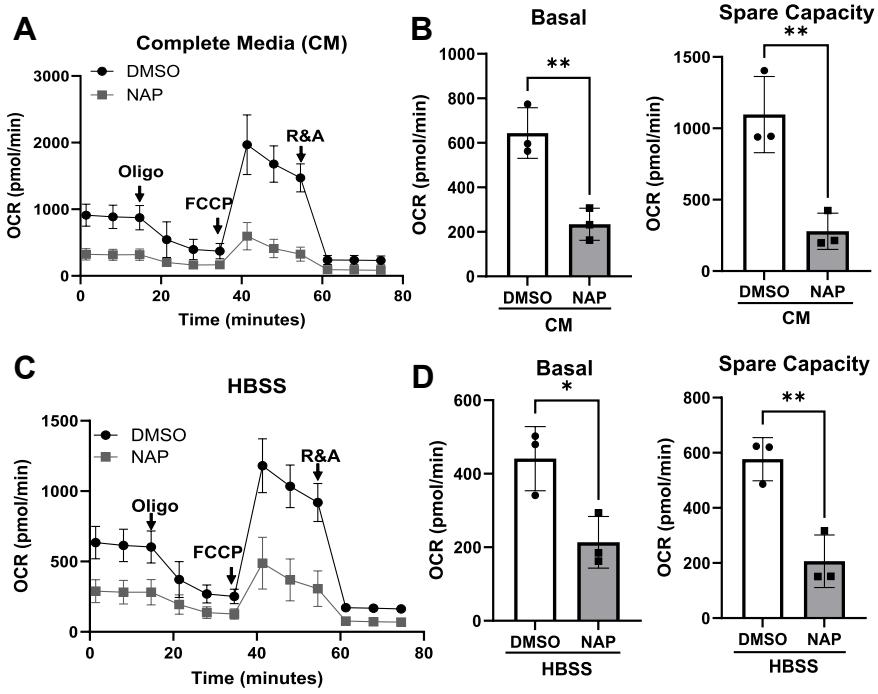


Figure 4. Inhibition of Rab5 decreases HCC energy homeostasis. *A*, Seahorse metabolic analysis showing NAP (100 μM, 48 h) inhibition of Rab5 decreases oxygen consumption rate (OCR) compared with control in complete media. n = 3 independent experiments. *B*, quantification of basal and spare respiratory capacity in complete media following treatment with NAP. *C*, Seahorse metabolic analysis showing DMSO *versus* NAP treatment in Hep3B cells under 4 h HBSS starvation. *D*, quantification of basal and spare respiratory capacity from *C*. *Graphs* represent mean ± SD from n = 3 independent experiments. Statistical significance was determined using an unpaired two-tailed *t* test. *$p < 0.05$, **$p < 0.01$. DMSO, dimethyl sulfoxide; HBSS, Hank's balanced salt solution; HCC, hepatocellular carcinoma; NAP, neoandrographolide.

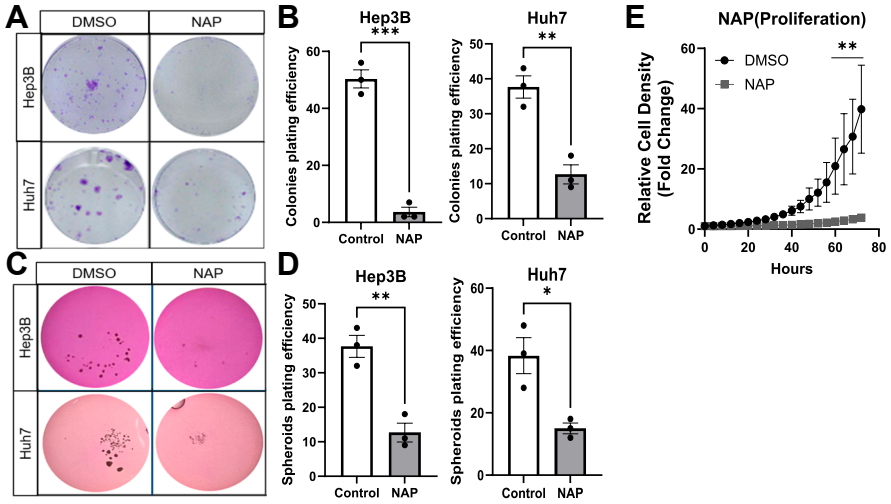


Figure 5. NAP treatment decreases HCC cell proliferation. *A*, representative images and quantification (*B*) showing colony formation assay of Hep3B and Huh7 cells treated with NAP (50 μM) for 12 days. *C*, spheroid formation assay of Huh7 and Hep3B cells treated with NAP (50 μM) for 5 days. *D*, quantification of spheroid formation assay from n = 3 independent experiments. *E*, quantification of IncuCyte live-cell imaging of Hep3B cells treated with DMSO (vehicle control) or NAP (100 μM), and relative cell density (fold change) was monitored over 72 h. *Graphs* represent mean ± SD from n = 3 independent experiments. Statistical significance was determined using an unpaired two-tailed *t* test. $*p < 0.05$, $**p < 0.01$, and $***p < 0.001$. DMSO, dimethyl sulfoxide; HCC, hepatocellular carcinoma; NAP, neoandrographolide.

exhibited robust colony growth, forming an average of ∼40 to 55 colonies per well in both Hep3B and Huh7 lines. In contrast, treatment with NAP significantly reduced colony numbers by ∼80% to 90% compared with untreated controls (Fig. 5*B*), indicating a possible role for Rab5 GTP–binding activity in sustaining clonal proliferation of HCC cells. Consistent with the 2D colony results, Rab5 inhibition markedly reduced 3D spheroid size and number in Hep3B and Huh7 cells as compared with controls (Fig. 5*C*). While control cells formed large, dense spheroids indicative of high proliferative and metabolic capacity, NAP-treated cells showed reduced spheroid formation, reflecting impaired self-renewal and growth potential. To determine if these effects were due to cytotoxicity, we performed 72 h of 3-(4,5-dimethylthiazol-2-yl)-2,5-diphenyltetrazolium bromide (MTT) dose–response assays at increasing concentrations of NAP. These results showed that NAP reduced viability with IC_{50} values of ∼249 μM in Hep3B and ∼500 μM in Huh7 cells (Fig. S4, *A* and *B*), far higher than the concentrations used for colony formation (50 μM) and spheroid assays (100 μM). Together, these findings suggest that Rab5-driven LD catabolism may support not only energy homeostasis (Figs. 5 and 6) but also the clonogenic and tumorigenic potential of HCC cells.

To further assess the impact of Rab5 inhibition on HCC cell growth, we performed a real-time proliferation assay using IncuCyte live-cell imaging for 72 h (Fig. 5*E*). Cells treated with NAP showed near-complete suppression of proliferation compared with DMSO controls, with minimal increase in cell density over time. These findings indicate that Rab5 activity is not only essential for maintaining lipid metabolism and mitochondrial function but also for driving HCC cell expansion.

Rab5 overexpression in HCC indicates adverse clinical outcomes

Rab5 exists as three isoforms (A, B, and C) on separate gene loci, although each isoform possesses ∼80% sequence homology. To investigate the differential expression of Rab5 isoforms and other known LD-associated proteins in patient HCC samples, we conducted a transcriptomic analysis using publicly available datasets from Gene Expression Omnibus, Genotype-Tissue Expression, The Cancer Genome Atlas, and TARGET projects. These datasets collectively include gene expression profiles from both tumors and adjacent normal liver tissues, providing a comprehensive view of transcriptional changes associated with liver tumorigenesis. A curated gene list of known LD-associated proteins was compiled to assess their expression dynamics in HCC (26). Analysis of this dataset revealed that RAB5A, RAB5B, and RAB5C were all significantly upregulated in HCC tumors compared with adjacent normal tissue (Fig. 6*A*, Table S1) (26, 47).

To assess Rab5 protein levels in human liver tissue, we examined a liver tissue microarray containing a small cohort of normal liver and HCC specimens. Immunohistochemistry revealed weak Rab5 staining in normal liver but markedly stronger cytoplasmic staining in HCC tissues (Fig. 6*B*). Semiquantitative pathology scores were significantly higher in HCC samples than in normal liver (Fig. 6*C*), indicating that Rab5 upregulation is also evident at the protein level in human HCC.

To identify core oncogenic processes that are most closely associated with elevated Rab5 expression in cancer, we utilized a previously curated list of cancer hallmark gene sets derived from the integrated cancer hallmark gene set assembled from the catalog of somatic mutations in cancer and curated literature sources for enrichment analysis using

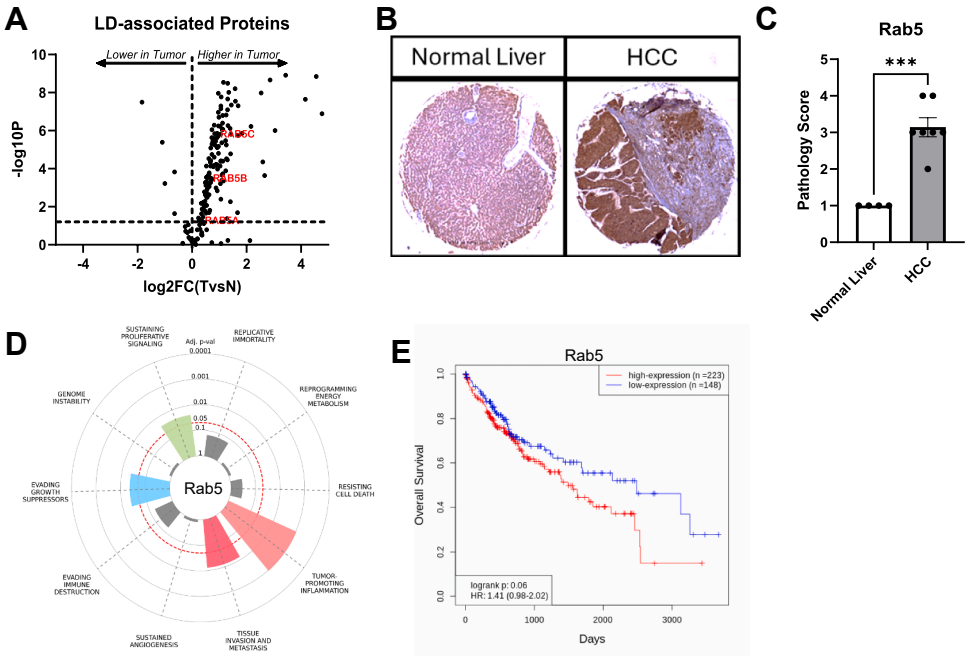


Figure 6. Rab5 is upregulated in HCC and associated with cancer hallmarks. *A*, volcano plot from TNMplot showing expression of known lipid droplet (LD)–associated proteins, including Rab5A/B/C, in HCC tumors *versus* adjacent normal tissues from n = 53 patients. *B*, representative immunohistochemistry images from a liver tissue microarray showing Rab5 staining in normal liver (n = 4) *versus* HCC specimens (n = 7). *C*, quantification of Rab5 immunohistochemistry scores from the tissue microarray (mean ± SD, ***$p < 0.0002$; Welch's *t* test). *D*, cancer hallmark gene set enrichment analysis based on the study by Menyhart *et al.* (48), showing Rab5-associated genes enriched in proliferation, invasion, and evading growth suppressors. *E*, Kaplan–Meier survival analysis from the TCGA–LIHC dataset stratified by Rab5 expression. High Rab5 expression correlates with poorer overall survival (log-rank test, $p = 0.06$). HCC, hepatocellular carcinoma; LIHC, Liver Hepatocellular Carcinoma Cohort; TCGA, The Cancer Genome Atlas.

the 10 canonical "Hallmarks of Cancer" (Table S1) (48). For each hallmark, we quantified the overlap between Rab5-associated genes and hallmark gene sets and assessed statistical significance using *p* values, false discovery rate–adjusted *p* values, and fold enrichment (odds ratio) (48). The circular bar chart (Fig. 6*D*) and hallmark over-representation table (Table S2) highlight enrichment of Rab5-associated genes in tumor-promoting inflammation, invasion and metastasis, evasion of growth suppressors, and sustained proliferative signaling. Conversely, little to no enrichment is seen for genome instability, sustained angiogenesis, and reprogramming energy metabolism, suggesting putative roles for Rab5 in proliferative and invasive pathways in cancer.

We also performed Kaplan–Meier survival analysis, which incorporates clinical outcome data from over 10,000 cancer patients in the The Cancer Genome Atlas study and corresponding normal tissue data from the Genotype-Tissue Expression project. Patients were stratified into high- and low-RAB5A expression groups based on the median expression level. The results (Fig. 6*E*) suggest that Rab5 expression may be associated with worse outcomes in univariate analysis, consistent with previous studies (49, 50). Overall, these integrated analyses encompassing differential expression, hallmark enrichment, and survival correlations suggest that Rab5 may be upregulated in HCC and play a role in core oncogenic processes, such as proliferation and invasion, potentially worsening patient outcomes. These findings support Rab5 as a biologically relevant contributor to tumor cell proliferation (Fig. 7) and may serve as a candidate therapeutic target warranting further validation, although likely not an independent prognostic factor.

Discussion

LD catabolism provides essential fuel for tumor growth and survival under metabolic stress across multiple cancer types (51), yet the molecular regulators and trafficking pathways that govern LD degradation in HCC remain poorly characterized. The data presented here support a model in which nutrient deprivation activates Rab5 to promote its recruitment to LDs, possibly promoting microlipophagic degradation and sustaining mitochondrial β-oxidation to support HCC proliferation. Treatment with the Rab5 GTP–binding inhibitor NAP leads to LD accumulation, diminishes mitochondrial respiration, and abrogates both 2D colony and 3D spheroid growth as well as cell proliferation.

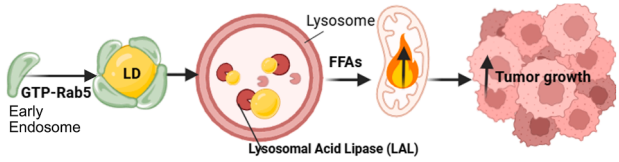


Figure 7. Working model depicting Rab5-mediated lipid droplet (LD) catabolism in HCC. Under nutrient deprivation, Rab5 GTP binding is increased and promotes a higher frequency of interaction with LDs, driving tethering and fusion with lysosomes *via* microlipophagy. Inside the lysosome, lysosomal acid lipase (LAL) degrades LD, releasing free fatty acids (FFAs), which are then shuttled to mitochondria for β-oxidation to fuel HCC cell proliferation and survival. HCC, hepatocellular carcinoma.

Nutrient deprivation activates several Rab GTPases as frontline responders to metabolic stress (43, 52, 53). Our group previously demonstrated that LD trafficking to lysosomes relies on Rab5-dependent endosomal microlipophagy rather than autophagosome-dependent macrolipophagy (13). The current study extends these findings in several important ways. First, we show that GTP-bound Rab5 exhibits a more pronounced localization to LDs (Fig. 1), in line with prior *in vitro* studies showing Rab5 on LDs in the presence of the nonhydrolyzable GTP analog GTPγS (36, 54). Under HBSS starvation, we observed a ∼50% increase in Rab5 GTP loading and an approximately threefold increase in LD recruitment (Fig. 2), consistent with previous reports showing Rab5 activation during serum withdrawal (55, 56). A recent study further demonstrated that amino acid withdrawal increases the colocalization of BODIPY-stained LDs with Rab5-positive endosomal compartments, indicating that nutrient stress brings Rab5-bearing membranes into close apposition with LDs (57). Interestingly, other Rab GTPases are also activated during nutrient starvation to stimulate lipophagy. For example, Rab7 is strongly GTP loaded under starvation to orchestrate lysosome-mediated LD degradation (52) and Rab10 is similarly activated to facilitate LD engulfment during lipophagy (43). In yeast, the Rab5 paralog Ypt53 is transcriptionally upregulated under nitrogen deprivation to boost endosomal trafficking and vacuolar activity (53). It is plausible that similar Rab5 activation may occur in tumor cells within the HCC tumor microenvironment, which is marked by limited nutrients and oxygen (58–60). Emerging evidence indicates that lipophagy may be a predominant route for LD degradation in hepatocytes (41, 61–63) under nutrient starvation or stress (61, 63). In support of this, liver-specific Rab5 knockdown in mice leads to marked LD accumulation and impaired mitochondrial β-oxidation (64), suggesting Rab5 plays a role in lipid catabolism. Consistent with these observations, we showed that disrupting Rab5's nucleotide cycle using NAP results in the accumulation of LDs, indicating impaired LD clearance (Fig. 3). In addition, we reveal that Rab5 inhibition reduces mitochondrial respiration in Hep3B cells, suggesting Rab5 may promote β-oxidation of LD-derived fatty acids (Fig. 4, *A–D*). Under both nutrient-replete and nutrient-deprived conditions, Rab5 inhibition with NAP causes a marked reduction in mitochondrial respiration, demonstrating that, even when external fuels are abundant, HCC cells may utilize Rab5-driven LD catabolism to fuel mitochondrial oxidation of intracellular lipid stores. Functionally, Rab5 inhibition profoundly impairs cell proliferation (Fig. 5, *A–E*), consistent with previous studies showing NAP treatment suppresses growth of lung cancer cells *via* inhibition of Rab5 GTP binding (44). Given our somewhat limited knowledge of NAP specificity, our data may support Rab5 as a potential therapeutic target but warrant further investigation as a definitive anti-Rab5 drug for HCC.

Cancer cells reorganize the Rab GTPase network to support increased membrane trafficking, nutrient uptake, and survival. Our transcriptomic and tissue microarray analyses (Fig. 6) suggest an upregulation of Rab5 within HCC tumors that may impact patient survival (65–68). While the transcriptional mechanisms that govern Rab5 overexpression in HCC remain undefined, we postulate this may be driven by a convergence of oncogenic growth factor signaling, hypoxia-induced pathways, and nutrient stress in tumor cells. Overall, the current study supports a possible link between Rab5 expression and liver tumor pathology.

Despite evidence that NAP inhibits mitochondrial respiration and potentially blocks LD clearance in HCC cells, several caveats are worth further consideration. First, although NAP is reported to inhibit Rab5 GTPase activity, it may also disrupt other Rab5-dependent processes or have off-target effects, such as clathrin-mediated endocytosis, macropinocytic nutrient uptake, general autophagy initiation, multivesicular body biogenesis, and integrin recycling, thereby broadly impairing cellular signaling, cell migration, and adhesion (39, 56, 69–77). Accordingly, we interpret our pharmacologic data with caution and view them in the context of our prior genetic work showing that Rab5 knockdown in HepG2 HCC cells causes robust LD accumulation and impaired microlipophagy, consistent with key aspects of NAP treatment (13). Second, acute HBSS treatment deprives cells of multiple nutrients and can nonspecifically suppress mitochondrial respiration and activate global autophagy programs, making it challenging to isolate Rab5-specific lipophagic effects. Third, while lipophagy is likely the dominant LD catabolic route in hepatocytes, we cannot rule out a possible role for Rab5 in macroautophagy, macrolipophagy, or neutral lipolysis *via* adipose triglyceride lipase/hormone-sensitive lipase (46). Furthermore, a dedicated fatty acid oxidation assay using exogenous fatty acid substrates (*e.g.*, bovine serum albumin [BSA]-conjugated palmitate with and without etomoxir) would strengthen our conclusion that Rab5 promotes β-oxidation of LD-derived fatty acids. Future studies will be needed to explicitly link Rab5 activity to fatty acid oxidation.

The nature of Rab5 interaction with LDs remains somewhat enigmatic, as it is unclear whether Rab5 binds directly to the LD monolayer or instead localizes indirectly *via* early endosomal membranes that dock onto LDs. In support of the latter possibility, a previous electron microscopy study has shown that transferrin–horseradish peroxidase–labeled early endosomal tubules form intimate contacts with LD surfaces (37), suggesting that Rab5 may reside on these endosomal membranes rather than embedding in the LD monolayer itself. However, this notion is challenged by our previous work showing that isolated LDs contain abundant levels of Rab5, yet seem to lack other early endosome markers, such as EEA1 (13). Nonetheless, our current working model is that Rab5 most likely influences microlipophagy through a population of Rab5-positive endosomes that physically associate with LDs to facilitate lipophagic flux.

The finding that Rab5 GTP binding is increased by nutrient starvation suggests that specific upstream nutrient-sensing kinases or guanine nucleotide exchange factors–GAPs may be responsible. For example, in muscle cells, AMP-activated protein kinase phosphorylates a Rab5-specific GAP to

increase Rab5 activity and promote GLUT4 translocation (69), raising the possibility that similar stress-activated kinases may govern Rab5 activation in hepatocytes. It would be interesting to probe similar nutrient kinases (AMP-activated protein kinase, mechanistic target of rapamycin) under HBSS or NAP treatment to further determine their impact on Rab5 activation during nutrient stress.

Within these limitations, our HBSS experiments help separate the role of starvation-driven lipophagy from the effects of Rab5 inhibition. During acute starvation, cells engage lipophagy to mobilize LD-stored fatty acids and maintain baseline ATP, but mitochondrial spare respiratory capacity remains low, and proliferation is unchanged (Fig. S2, *A–F*). This implies that lipophagy may support cell survival during nutrient stress, perhaps in addition to driving proliferation and ATP production. In contrast, pharmacologic Rab5 inhibition collapses LD utilization and β-oxidation even in nutrient-replete conditions, leading to impaired clonogenic and spheroid growth, indicating that starvation does not override the requirement for Rab5 in supporting rapid proliferation.

Transcriptomic analysis of human HCC tumor *versus* adjacent normal tissue shows an upregulation of all three Rab5 isoforms (Rab5A, Rab5B, and Rab5C) (Fig. 6*A*), but their individual contributions to lipid metabolism and tumor progression remain undefined. Although these isoforms share ∼80% sequence homology, other studies suggest that these isoforms can differ in localization, binding partners, and function (34, 78). Future studies will therefore employ isoform-specific CRISPR–Cas9 knockout or RNA interference to dissect their unique roles in lipophagy and HCC growth. Equally important is identifying the molecular effectors that link Rab5 to LD–lysosome trafficking; proximity-based proteomics (APEX/BioID) on isolated LDs could map the Rab5 interactome and reveal key tethering or fusion proteins. Finally, although we expanded our analyses beyond Hep3B and Huh7 to include additional cancer cell lines and a liver tissue microarray, our work remains limited to *in vitro* systems. It will be essential to validate Rab5's role and therapeutic potential using xenografts, genetically engineered mouse models, and patient-derived organoids in future studies.

Experimental procedures

Cell culture and reagents

Hep3B cells were cultured in minimum essential medium containing Earle's salts and L-glutamine, supplemented with 1 mM sodium pyruvate, nonessential amino acids, 0.075% (w/v) sodium bicarbonate, 10% fetal bovine serum, and 1% penicillin–streptomycin (Corning). Huh7 cells, MDA-MB-231 triple-negative breast cancer cells, and KPC8060 pancreatic ductal adenocarcinoma cells were maintained in Dulbecco's modified Eagle's medium supplemented with 10% fetal bovine serum, 1% penicillin–streptomycin, and 1% L-glutamine. All cells were grown in a humidified incubator at 37 °C with 5% CO_2. The primary antibodies obtained from Sigma–Aldrich and used in this study were anti-Actin (A2066) and anti-Myc tag (9B11). In addition, LDs were stained using ORO (O0625), also from Sigma–Aldrich. Antibodies against Rab5A (2143S), PLIN2 (95109), and EEA1 (2411S) were purchased from Cell Signaling Technology. OA (O1008) was also from Sigma–Aldrich. Critical antibodies were validated previously using siRNA knockdown approaches. Rab5 GTP binding was inhibited using NAP (Rab5 inhibitor, Cayman Chemical, 11742). The constitutively active GFP-Rab5 (Q79L) and dominant-negative GFP-Rab5 (S34N) constructs were gifted from Dr Sergio Grinstein (Addgene plasmids #35140 and #35141, respectively). The GFP-Rab5 was a gift from Marci Scidmore (Addgene plasmid #49888). In addition, Myc-tagged Rab5 was cloned in our laboratory into the pcDNA3.1Myc/His expression vector, and Myc-Rab5 (Q79L) and Myc-Rab5 (S34N) mutants were generated using site-directed mutagenesis. All constructs were confirmed by Sanger sequencing. All WT and mutant Rab5 constructs (GFP-Rab5 WT, Q79L, S34N, and the corresponding Myc-tagged versions) are based on human Rab5A complementary DNA. Hep3B cells were transfected at 40% to 60% confluency using Lipofectamine 2000 (Thermo Fisher Scientific) and harvested 24 to 48 h later for downstream assays.

Fluorescence microscopy

Cells were rinsed twice with PBS and then fixed in 3% formaldehyde for 10 min at room temperature. To stain LDs, samples were immersed in 60% isopropanol for 30 s, incubated in ORO working solution (5 mg/ml in isopropanol, diluted to 60% in water) for 2.5 min, and washed again in 60% isopropanol for 30 s. Confocal images were captured on a Nikon NSPARC confocal and fluorescent microscope using a 60× oil-immersion objective (numerical aperture = 1.42). LD metrics, including droplet number, size, and total area per cell, as well as GFP-Rab5 colocalization, were quantified in ImageJ (National Institutes of Health). To quantify Rab5 abundance around LDs, LDs were segmented in ImageJ, and corresponding LD regions of interest (ROIs) were converted to peripheral, donut-shaped ROIs with a bandwidth of 0.5 μm using the "Make Band" function. Rab5 fluorescence intensity was measured within the band region, and cytoplasmic Rab5 intensity was drawn using a second, hand-drawn ROI. The Rab5–LD contact ratio was then calculated by dividing the band intensity of the Rab5 channel (GFP or Myc) by the cytoplasmic intensity of the same channel.

Immunofluorescence microscopy

Hep3B cells transfected with Myc-Rab5 were seeded onto glass coverslips and treated overnight (16 h) with 150 μM OA to promote LD accumulation. Cells were fixed with 3% formaldehyde at room temperature, permeabilized with 0.2% saponin, and blocked in saponin–BSA blocking buffer for 60 min at 37 °C. Coverslips were incubated with primary antibodies diluted in saponin–BSA buffer (200 μl per sample) for 1 h at 37 °C, washed, and then incubated with Alexa Fluor 488–conjugated secondary antibody (Invitrogen,

catalog –11008; 1:500 dilution) for 30 min at 37 °C, protected from light. LDs were visualized by ORO staining, and nuclei were labeled using ProLong Gold Antifade Reagent containing 4′,6-diamidino-2-phenylindole (Invitrogen).

GTP pull-down assay

Hep3B cells were harvested and lysed in GTP–agarose lysis/wash buffer (50 mM Tris–HCl, pH 7.5; 250 mM NaCl; 5 mM Mg acetate; 0.5% Triton X-100; protease inhibitors) (79). Lysates were clarified by centrifugation (13,000*g*, 10 min, 4 °C). A 50 μl aliquot of each supernatant was reserved as an input control. The remaining lysate (∼0.5–1 mg protein) was incubated with 300 μl GTP–agarose beads (Sigma; G9768) overnight at 4 °C with gentle rotation. Beads were washed in lysis buffer, eluted into Laemmli buffer, and boiled. Samples were resolved by SDS-PAGE and analyzed by Western blot. All Western blots were visualized using enhanced chemiluminescence and developed on an autoradiography film. Band intensities were quantified using ImageJ software.

LD isolation

LDs were isolated from Hep3B cells cultured to approximately 90% confluency in 15 cm dishes (10 dishes per condition). To induce lipid accumulation, cells were treated with 150 μM OA for 16 h. LD isolation was performed using a modified protocol based on previously published methods (80, 81). In brief, cells were resuspended in a hypotonic lysis buffer and mechanically lysed using a Dounce homogenizer. The resulting postnuclear supernatant was carefully layered beneath a 30% to 0% OptiPrep density gradient (Sigma, D1556). Following centrifugation at 17,200 rpm for 30 min with the SW55Ti rotor at 4 °C, the lipid-rich fraction that floated to the top was collected. Isolated LDs were washed and prepared for downstream analysis by Western blot. PLIN2 served as an LD-specific loading control.

Seahorse metabolic analysis

To assess mitochondrial function, adherent cells were seeded at a density of 3×10^4 cells per well in a Seahorse XF96 Cell Culture Microplate (Agilent Technologies), using cell line–specific standard growth media. Each experimental group consisted of 10 technical replicates. To ensure even cell distribution, the plates were left undisturbed at room temperature for 20 min before being incubated overnight at 37 °C to allow for proper cell attachment. On the following day, the culture medium was replaced with Seahorse XF Base Medium (Phenol Red–free Dulbecco's modified Eagle's medium), and the Cell Mito Stress Test (Agilent) was performed in accordance with the manufacturer's protocol. After sensor calibration, the assay involved a series of injections with the following compounds to evaluate mitochondrial respiration: oligomycin A (1.5 μM) to inhibit ATP synthase, carbonyl cyanide-*p*-trifluoromethoxyphenylhydrazone (1.0 μM) to uncouple oxidative phosphorylation, and a mixture of rotenone and antimycin A (0.5 μM) to inhibit complex I and III, respectively. Following the Seahorse assay, cells were lysed using radioimmunoprecipitation assay buffer, and protein concentration was determined *via* bicinchoninic acid assay. The measured protein content was used to normalize the OCR and other metabolic parameters from each well to ensure accurate data comparison.

Incucyte live-cell assay

Hep3B cells were seeded at a density of 3000 cells per well in 96-well plates (100 μl/well) using standard growth medium and incubated overnight at 37 °C in a humidified incubator with 5% CO_2. On the following day, the culture medium was aspirated and replaced with 100 μl of treatment medium containing IncuCyte Cytotox Green Reagent for real-time cell health analysis (#4633, Sartorius), prepared according to the manufacturer's protocol. Plates were loaded into the IncuCyte S3 Live-Cell Analysis System (Essen BioScience) and allowed to equilibrate at 37 °C for 30 min before imaging. Time-lapse images were acquired every 3 to 4 h using a 10x objective in both phase contrast and green fluorescence channels. Cell proliferation was monitored using phase-contrast imaging to measure confluence over time. All image acquisition and analysis were performed using the IncuCyte integrated cell-by-cell analysis module, allowing for high-content quantification of both viability and growth dynamics at single-cell resolution.

Colony and spheroid formation assays

To assess both 2D and 3D growth capacities, Hep3B and Huh7 cells were subjected to colony and spheroid formation assays under identical treatment conditions. For the colony formation assay, cells were seeded at 80 cells per well in 24-well plates and allowed to attach for 16 h. Treatments with 50 μM NAP or DMSO (vehicle control) were applied and maintained for 12 days, with media refreshed as necessary. Colonies were fixed in methanol, stained with 0.5% crystal violet for 5 min, rinsed with water, and air dried. Colony number and size were quantified using ImageJ software (82). For the spheroid formation assay, 600 cells per well were seeded into Spherical 5D microwell plates and allowed to aggregate overnight. The resulting cell aggregates were then transferred to CelVivo clinoreactor plates and cultured under identical treatment conditions for 5 days. Spheroids were subsequently collected into standard 6-well plates and imaged for morphological analysis.

Tissue microarray and immunohistochemistry

Rab5 protein expression was assessed using a commercially available liver tissue microarray (LV483a; US Biomax, Inc) containing normal liver and HCC specimens. Formalin-fixed, paraffin-embedded sections were stained with an anti-Rab5 primary antibody (Cell Signaling Technology, 3547) followed by standard immunohistochemistry detection procedures. A pathologist evaluated staining intensity and distribution, and semiquantitative Rab5 expression scores were generated for all samples containing normal liver and HCC specimens.

ASBMB

MTT cell viability assay

Cell viability was measured using a 72 h MTT assay. Hep3B and Huh7 cells were seeded in 96-well plates at a density of 1.5×10^3 cells per well and allowed to adhere overnight in CM. Cells were then treated with increasing concentrations of NAP (0–1000 μM) or DMSO vehicle control for 72 h. At the end of the treatment period, MTT reagent (0.5 mg/ml final concentration) was added to each well and incubated for 3 to 4 h at 37 °C to allow formation of formazan crystals. The medium was then carefully removed, and the formazan product was solubilized in DMSO (or MTT solvent) with gentle shaking for 10 to 15 min. Absorbance at 570 nm was measured using a microplate reader, and background was subtracted using a reference wavelength (*e.g.*, 630–690 nm) when* applicable. Relative cell viability was calculated by normalizing absorbance values to DMSO-treated controls, and IC_{50} values were determined from dose–response curves using nonlinear regression analysis.

Data availability

All data are contained within the article and are available from the corresponding author upon reasonable request.

Supporting information—This article contains supporting information.

Acknowledgments—We thank Dr Justin Mott and members of the Schott laboratory for helpful discussions, and we are grateful to Dr Manesh Jain and Dr Abhijit Aithal for access to the IncuCyte system. We also thank Dr Suyong Choi for generously providing the pancreatic ductal adenocarcinoma and triple-negative breast cancer cell lines used in this study. The graphical illustrations were created with BioRender.com.

Author contributions—K. O. O., M. A. A. Z., and M. B. S. conceptualization; M. B. S. methodology; K. O. O., M. A. A. Z., K. W. F., and M. B. S. formal analysis; K. O. O. and M. A. A. Z. investigation; K. O. O., M. A. A. Z., and K. W. F. data curation; K. O. O., M. A. A. Z., R. E. O.-D., M. P. P., and M. B. S. writing–original draft; K. O. O., M. A. A. Z., R. E. O.-D., M. P. P., K. W. F., and M. B. S. writing–review & editing; M. B. S. supervision; M. B. S. funding acquisition.

Funding and additional information—This work was supported by the National Cancer Institute R21 grant R21CA279878, the National Institute on Alcohol Abuse and Alcoholism, National Institutes of Health R00 grant R00AA026877, and the National Institute of General Medical Sciences, National Institutes of Health R35 MIRA Award R35GM150801 (to M. B. S.). The content is solely the responsibility of the authors and does not necessarily represent the official views of the National Institutes of Health.

Conflict of interest—The authors declare that they have no conflicts of interest with the contents of this article.

Abbreviations—The abbreviations used are: BSA, bovine serum albumin; CM, complete medium; DMSO, dimethyl sulfoxide; EEA1, early endosome antigen 1; GAP, GTPase-activating protein; HBSS, Hank's balanced salt solution; HCC, hepatocellular carcinoma; LD, lipid droplet; MTT, 3-(4,5-dimethylthiazol-2-yl)-2,5-diphenyltetrazolium bromide; NAP, neoandrographolide; OA, oleic acid; OCR, oxygen consumption rate; ORO, Oil Red O; PLIN-2, perilipin-2; ROI, region of interest.

References

1. Yarchoan, M., Agarwal, P., Villanueva, A., Rao, S., Dawson, L. A., Llovet, J. M., *et al.* (2019) Recent developments and therapeutic strategies against hepatocellular carcinoma. *Cancer Res.* **79**, 4326–4330
2. Samant, H., Amiri, H. S., and Zibari, G. B. (2021) Addressing the worldwide hepatocellular carcinoma: epidemiology, prevention and management. *J. Gastrointest. Oncol.* **12**, S361–s373
3. Gao, Y. X., Ning, Q. Q., Yang, P. X., Guan, Y. Y., Liu, P. X., Liu, M. L., *et al.* (2023) Recent advances in recurrent hepatocellular carcinoma therapy. *World J. Hepatol.* **15**, 460–476
4. Yilma, M., Houhong Xu, R., Saxena, V., Muzzin, M., Tucker, L. Y., Lee, J., *et al.* (2024) Survival outcomes among patients with hepatocellular carcinoma in a large integrated US health system. *JAMA Netw. Open* **7**, e2435066
5. Loomba, R., Yang, H. I., Su, J., Brenner, D., Barrett-Connor, E., Iloeje, U., *et al.* (2013) Synergism between obesity and alcohol in increasing the risk of hepatocellular carcinoma: a prospective cohort study. *Am. J. Epidemiol.* **177**, 333–342
6. Liu, Y., Sun, Z., Wang, Q., Wu, K., Tang, Z., and Zhang, B. (2023) Contribution of alcohol use to the global burden of cirrhosis and liver cancer from 1990 to 2019 and projections to 2044. *Hepatol. Int.* **17**, 1028–1044
7. Julien, J., Ayer, T., Tapper, E. B., Barbosa, C., Dowd, W. N., and Chhatwal, J. (2022) Effect of increased alcohol consumption during COVID-19 pandemic on alcohol-associated liver disease: a modeling study. *Hepatology* **75**, 1480–1490
8. Thrift, A. P., Kanwal, F., Lim, H., Duong, H., Liu, Y., Singal, A. G., *et al.* (2024) PNPLA3, obesity, and heavy alcohol use in cirrhosis patients may exert a synergistic increase hepatocellular carcinoma risk. *Clin. Gastroenterol. Hepatol.* **22**, 1858–1866.e1854
9. Ghazanfar, H., Javed, N., Qasim, A., Zacharia, G. S., Ghazanfar, A., Jyala, A., *et al.* (2024) Metabolic dysfunction-associated steatohepatitis and progression to hepatocellular carcinoma: a literature review. *Cancers (Basel)* **16**, 1214
10. Younossi, Z. M., Kalligeros, M., and Henry, L. (2025) Epidemiology of metabolic dysfunction-associated steatotic liver disease. *Clin. Mol. Hepatol.* **31**, S32–S50
11. Sangineto, M., Villani, R., Cavallone, F., Romano, A., Loizzi, D., and Serviddio, G. (2020) Lipid metabolism in development and progression of hepatocellular carcinoma. *Cancers (Basel)* **12**, 1419
12. Li, B., Li, Y., Zhou, H., Xu, Y., Cao, Y., Cheng, C., *et al.* (2024) Multiomics identifies metabolic subtypes based on fatty acid degradation allocating personalized treatment in hepatocellular carcinoma. *Hepatology* **79**, 289–306
13. Schott, M. B., Rozeveld, C. N., Bhatt, S., Crossman, B., Krueger, E. W., Weller, S. G., *et al.* (2024) Ethanol disrupts hepatocellular lipophagy by altering Rab5-centric LD-lysosome trafficking. *Hepatol. Commun.* **8**, e0446
14. Kumar, R., Arrowood, C., Schott, M. B., and Nazarko, T. Y. (2025) Microlipophagy from simple to complex eukaryotes. *Cells* **14**, 141
15. Vevea, J. D., Garcia, E. J., Chan, R. B., Zhou, B., Schultz, M., Di Paolo, G., *et al.* (2015) Role for lipid droplet biogenesis and microlipophagy in adaptation to lipid imbalance in yeast. *Dev. Cell* **35**, 584–599
16. van Zutphen, T., Todde, V., de Boer, R., Kreim, M., Hofbauer, H. F., Wolinski, H., *et al.* (2014) Lipid droplet autophagy in the yeast Saccharomyces cerevisiae. *Mol. Biol. Cell* **25**, 290–301
17. Wang, C. W., Miao, Y. H., and Chang, Y. S. (2014) A sterol-enriched vacuolar microdomain mediates stationary phase lipophagy in budding yeast. *J. Cell Biol.* **206**, 357–366
18. Schulze, R. J., Krueger, E. W., Weller, S. G., Johnson, K. M., Casey, C. A., Schott, M. B., *et al.* (2020) Direct lysosome-based autophagy of lipid droplets in hepatocytes. *Proc. Natl. Acad. Sci. U. S. A.* **117**, 32443–32452

19. Robichaud, S., Fairman, G., Vijithakumar, V., Mak, E., Cook, D. P., Pelletier, A. R., *et al.* (2021) Identification of novel lipid droplet factors that regulate lipophagy and cholesterol efflux in macrophage foam cells. *Autophagy* **17**, 3671–3689
20. Zhao, P., Tian, R., Song, D., Zhu, Q., Ding, X., Zhang, J., *et al.* (2025) Rab GTPases are evolutionarily conserved signals mediating selective autophagy. *J. Cell Biol.* **224**, e202410150
21. Maan, M., Peters, J. M., Dutta, M., and Patterson, A. D. (2018) Lipid metabolism and lipophagy in cancer. *Biochem. Biophys. Res. Commun.* **504**, 582–589
22. Kounakis, K., Chaniotakis, M., Markaki, M., and Tavernarakis, N. (2019) Emerging roles of lipophagy in health and disease. *Front. Cell Dev. Biol.* **7**, 185
23. Brasaemle, D. L., Dolios, G., Shapiro, L., and Wang, R. (2004) Proteomic analysis of proteins associated with lipid droplets of basal and lipolytically stimulated 3T3-L1 adipocytes. *J. Biol. Chem.* **279**, 46835–46842
24. Cermelli, S., Guo, Y., Gross, S. P., and Welte, M. A. (2006) The lipid-droplet proteome reveals that droplets are a protein-storage depot. *Curr. Biol.* **16**, 1783–1795
25. Sato, S., Fukasawa, M., Yamakawa, Y., Natsume, T., Suzuki, T., Shoji, I., *et al.* (2006) Proteomic profiling of lipid droplet proteins in hepatoma cell lines expressing hepatitis C virus core protein. *J. Biochem.* **139**, 921–930
26. Bersuker, K., Peterson, C. W. H., To, M., Sahl, S. J., Savikhin, V., Grossman, E. A., *et al.* (2018) A proximity labeling strategy provides insights into the composition and dynamics of lipid droplet proteomes. *Dev. Cell* **44**, 97–112.e117
27. Zhang, H., Wang, Y., Li, J., Yu, J., Pu, J., Li, L., *et al.* (2011) Proteome of skeletal muscle lipid droplet reveals association with mitochondria and apolipoprotein a-I. *J. Proteome Res.* **10**, 4757–4768
28. Martinez-Arroyo, O., Selma-Soriano, E., Ortega, A., Cortes, R., and Redon, J. (2021) Small rab GTPases in intracellular vesicle trafficking: the case of Rab3A/Raphillin-3A complex in the kidney. *Int. J. Mol. Sci.* **22**, 7679
29. Stenmark, H., Parton, R. G., Steele-Mortimer, O., Lütcke, A., Gruenberg, J., and Zerial, M. (1994) Inhibition of rab5 GTPase activity stimulates membrane fusion in endocytosis. *EMBO J.* **13**, 1287–1296
30. Park, M. H., Choi, K. Y., and Min do, S. (2015) The pleckstrin homology domain of phospholipase D1 accelerates EGFR endocytosis by increasing the expression of the Rab5 effector, rabaptin-5. *Exp. Mol. Med.* **47**, e200
31. Yuan, W., and Song, C. (2020) The emerging role of Rab5 in membrane receptor trafficking and signaling pathways. *Biochem. Res. Int.* **2020**, 4186308
32. Pfeffer, S. R. (2013) Rab GTPase regulation of membrane identity. *Curr. Opin. Cell Biol.* **25**, 414–419
33. Lawe, D. C., Chawla, A., Merithew, E., Dumas, J., Carrington, W., Fogarty, K., *et al.* (2002) Sequential roles for phosphatidylinositol 3-phosphate and Rab5 in tethering and fusion of early endosomes via their interaction with EEA1. *J. Biol. Chem.* **277**, 8611–8617
34. Rastogi, R., Verma, J. K., Kapoor, A., Langsley, G., and Mukhopadhyay, A. (2016) Rab5 isoforms specifically regulate different modes of endocytosis in Leishmania. *J. Biol. Chem.* **291**, 14732–14746
35. Saitoh, S., Maruyama, T., Yako, Y., Kajita, M., Fujioka, Y., Ohba, Y., *et al.* (2017) Rab5-regulated endocytosis plays a crucial role in apical extrusion of transformed cells. *Proc. Natl. Acad. Sci. U. S. A.* **114**, E2327–e2336
36. Liu, P., Bartz, R., Zehmer, J. K., Ying, Y. S., Zhu, M., Serrero, G., *et al.* (2007) Rab-regulated interaction of early endosomes with lipid droplets. *Biochim. Biophys. Acta* **1773**, 784–793
37. Parton, R. G., Bosch, M., Steiner, B., and Pol, A. (2020) Novel contact sites between lipid droplets, early endosomes, and the endoplasmic reticulum. *J. Lipid Res.* **61**, 1364
38. Zhou, F., Zou, S., Chen, Y., Lipatova, Z., Sun, D., Zhu, X., *et al.* (2017) A Rab5 GTPase module is important for autophagosome closure. *PLoS Genet.* **13**, e1007020
39. Hammerling, B. C., Najor, R. H., Cortez, M. Q., Shires, S. E., Leon, L. J., Gonzalez, E. R., *et al.* (2017) A Rab5 endosomal pathway mediates Parkin-dependent mitochondrial clearance. *Nat. Commun.* **8**, 14050
40. Zhou, F., Wu, Z., Zhao, M., Murtazina, R., Cai, J., Zhang, A., *et al.* (2019) Rab5-dependent autophagosome closure by ESCRT. *J. Cell Biol.* **218**, 1908–1927
41. Schott, M. B., Weller, S. G., Schulze, R. J., Krueger, E. W., Drizyte-Miller, K., Casey, C. A., *et al.* (2019) Lipid droplet size directs lipolysis and lipophagy catabolism in hepatocytes. *J. Cell Biol.* **218**, 3320–3335
42. Rambold, A. S., Cohen, S., and Lippincott-Schwartz, J. (2015) Fatty acid trafficking in starved cells: regulation by lipid droplet lipolysis, autophagy, and mitochondrial fusion dynamics. *Dev. Cell* **32**, 678–692
43. Li, Z., Schulze, R. J., Weller, S. G., Krueger, E. W., Schott, M. B., Zhang, X., *et al.* (2016) A novel Rab10-EHBP1-EHD2 complex essential for the autophagic engulfment of lipid droplets. *Sci. Adv.* **2**, e1601470
44. Zhang, J., Sun, Y., Zhong, L. Y., Yu, N. N., Ouyang, L., Fang, R. D., *et al.* (2020) Structure-based discovery of neoandrographolide as a novel inhibitor of Rab5 to suppress cancer growth. *Comput. Struct. Biotechnol. J.* **18**, 3936–3946
45. van der Windt, G. J., Everts, B., Chang, C. H., Curtis, J. D., Freitas, T. C., Amiel, E., *et al.* (2012) Mitochondrial respiratory capacity is a critical regulator of CD8+ T cell memory development. *Immunity* **36**, 68–78
46. Marchetti, P., Fovez, Q., Germain, N., Khamari, R., and Kluza, J. (2020) Mitochondrial spare respiratory capacity: mechanisms, regulation, and significance in non-transformed and cancer cells. *FASEB J* **34**, 13106–13124
47. Bartha, Á., and Győrffy, B. (2021) TNMplot.com: a web tool for the comparison of gene expression in normal, tumor and metastatic tissues. *Int. J. Mol. Sci.* **22**, 2622
48. Menyhart, O., Kothalawala, W. J., and Győrffy, B. (2025) A gene set enrichment analysis for cancer hallmarks. *J. Pharm. Anal* **15**, 101065
49. Tang, G., Liu, X., Cho, M., Li, Y., Tran, D. H., and Wang, X. (2024) Pan-cancer discovery of somatic mutations from RNA sequencing data. *Commun. Biol.* **7**, 619
50. Tang, G., Cho, M., and Wang, X. (2022) OncoDB: an interactive online database for analysis of gene expression and viral infection in cancer. *Nucleic Acids Res.* **50**, D1334–d1339
51. Munir, R., Lisec, J., Swinnen, J. V., and Zaidi, N. (2019) Lipid metabolism in cancer cells under metabolic stress. *Br. J. Cancer* **120**, 1090–1098
52. Schroeder, B., Schulze, R. J., Weller, S. G., Sletten, A. C., Casey, C. A., and McNiven, M. A. (2015) The small GTPase Rab7 as a central regulator of hepatocellular lipophagy. *Hepatology* **61**, 1896–1907
53. Nakatsukasa, K., Kanada, A., Matsuzaki, M., Byrne, S. D., Okumura, F., and Kamura, T. (2014) The nutrient stress-induced small GTPase Rab5 contributes to the activation of vesicle trafficking and vacuolar activity. *J. Biol. Chem.* **289**, 20970–20978
54. Stroupe, C., and Brunger, A. T. (2000) Crystal structures of a rab protein in its inactive and active conformations. *J. Mol. Biol.* **304**, 585–598
55. Dou, Z., Pan, J. A., Dbouk, H. A., Ballou, L. M., DeLeon, J. L., Fan, Y., *et al.* (2013) Class IA PI3K p110β subunit promotes autophagy through Rab5 small GTPase in response to growth factor limitation. *Mol. Cell* **50**, 29–42
56. Ravikumar, B., Imarisio, S., Sarkar, S., O'Kane, C. J., and Rubinsztein, D. C. (2008) Rab5 modulates aggregation and toxicity of mutant huntingtin through macroautophagy in cell and fly models of Huntington disease. *J. Cell Sci.* **121**, 1649–1660
57. Peng, W., Chen, S., Ma, J., Wei, W., Lin, N., Xing, J., *et al.* (2025) Endosomal trafficking participates in lipid droplet catabolism to maintain lipid Homeostasis. *Nat. Commun.* **16**, 1917
58. Tian, Y., Yang, B., Qiu, W., Hao, Y., Zhang, Z., Yang, B., *et al.* (2019) ER-residential Nogo-B accelerates NAFLD-associated HCC mediated by metabolic reprogramming of oxLDL lipophagy. *Nat. Commun.* **10**, 3391
59. Minami, S., Yamamoto, T., Takabatake, Y., Takahashi, A., Namba, T., Matsuda, J., *et al.* (2017) Lipophagy maintains energy homeostasis in the kidney proximal tubule during prolonged starvation. *Autophagy* **13**, 1629–1647
60. Peng, P., Chavel, C., Liu, W., Carlson, L. M., Cao, S., Utley, A., *et al.* (2024) Pro-survival signaling regulates lipophagy essential for multiple myeloma resistance to stress-induced death. *Cell Rep.* **43**, 114445

61. Cui, W., Sathyanarayan, A., Lopresti, M., Aghajan, M., Chen, C., and Mashek, D. G. (2021) Lipophagy-derived fatty acids undergo extracellular efflux via lysosomal exocytosis. *Autophagy* **17**, 690–705
62. Sathyanarayan, A., Mashek, M. T., and Mashek, D. G. (2017) ATGL promotes autophagy/lipophagy via SIRT1 to control hepatic lipid droplet catabolism. *Cell Rep.* **19**, 1–9
63. Singh, R., Kaushik, S., Wang, Y., Xiang, Y., Novak, I., Komatsu, M., *et al.* (2009) Autophagy regulates lipid metabolism. *Nature* **458**, 1131–1135
64. Zeigerer, A., Bogorad, R. L., Sharma, K., Gilleron, J., Seifert, S., Sales, S., *et al.* (2015) Regulation of liver metabolism by the endosomal GTPase Rab5. *Cell Rep.* **11**, 884–892
65. Frittoli, E., Palamidessi, A., Marighetti, P., Confalonieri, S., Bianchi, F., Malinverno, C., *et al.* (2014) A RAB5/RAB4 recycling circuitry induces a proteolytic invasive program and promotes tumor dissemination. *J. Cell Biol.* **206**, 307–328
66. Yu, M. H., Luo, Y., Qin, S. L., and Zhong, M. (2015) Increased expression of Rab5A predicts metastasis and poor prognosis in colorectal cancer patients. *Int. J. Clin. Exp. Pathol.* **8**, 6974–6980
67. Jian, Z., Zhang, L., Jin, L., Lan, W., Zhang, W., and Gao, G. (2020) Rab5 regulates the proliferation, migration and invasion of glioma cells via cyclin. *E Oncol. Lett.* **20**, 1055–1062
68. Igarashi, T., Araki, K., Yokobori, T., Altan, B., Yamanaka, T., Ishii, N., *et al.* (2017) Association of RAB5 overexpression in pancreatic cancer with cancer progression and poor prognosis via E-cadherin suppression. *Oncotarget* **8**, 12290–12300
69. Rao, X. S., Cong, X. X., Gao, X. K., Shi, Y. P., Shi, L. J., Wang, J. F., *et al.* (2021) AMPK-mediated phosphorylation enhances the auto-inhibition of TBC1D17 to promote Rab5-dependent glucose uptake. *Cell Death Differ* **28**, 3214–3234
70. Lakadamyali, M., Rust, M. J., and Zhuang, X. (2006) Ligands for clathrin-mediated endocytosis are differentially sorted into distinct populations of early endosomes. *Cell* **124**, 997–1009
71. Schnatwinkel, C., Christoforidis, S., Lindsay, M. R., Uttenweiler-Joseph, S., Wilm, M., Parton, R. G., *et al.* (2004) The Rab5 effector Rabankyrin-5 regulates and coordinates different endocytic mechanisms. *PLoS Biol.* **2**, E261
72. Silva, P., Mendoza, P., Rivas, S., Díaz, J., Moraga, C., Quest, A. F., *et al.* (2016) Hypoxia promotes Rab5 activation, leading to tumor cell migration, invasion and metastasis. *Oncotarget* **7**, 29548–29562
73. Maxson, M. E., Sarantis, H., Volchuk, A., Brumell, J. H., and Grinstein, S. (2021) Rab5 regulates macropinocytosis by recruiting the inositol 5-phosphatases OCRL and Inpp5b that hydrolyse PtdIns(4,5)P2. *J. Cell Sci.* **134**, jcs252411
74. Zeigerer, A., Gilleron, J., Bogorad, R. L., Marsico, G., Nonaka, H., Seifert, S., *et al.* (2012) Rab5 is necessary for the biogenesis of the endolysosomal system in vivo. *Nature* **485**, 465–470
75. Pellinen, T., Arjonen, A., Vuoriluoto, K., Kallio, K., Fransen, J. A., and Ivaska, J. (2006) Small GTPase Rab21 regulates cell adhesion and controls endosomal traffic of beta1-integrins. *J. Cell Biol.* **173**, 767–780
76. Torres, V. A., Mielgo, A., Barbero, S., Hsiao, R., Wilkins, J. A., and Stupack, D. G. (2010) Rab5 mediates caspase-8-promoted cell motility and metastasis. *Mol. Biol. Cell* **21**, 369–376
77. Torres, V. A., and Stupack, D. G. (2011) Rab5 in the regulation of cell motility and invasion. *Curr. Protein Pept. Sci.* **12**, 43–51
78. Chen, P. I., Kong, C., Su, X., and Stahl, P. D. (2009) Rab5 isoforms differentially regulate the trafficking and degradation of epidermal growth factor receptors. *J. Biol. Chem.* **284**, 30328–30338
79. Pensalfini, A., Kim, S., Subbanna, S., Bleiwas, C., Goulbourne, C. N., Stavrides, P. H., *et al.* (2020) Endosomal dysfunction induced by directly overactivating Rab5 recapitulates prodromal and neurodegenerative features of Alzheimer's disease. *Cell Rep.* **33**, 108420
80. Brasaemle, D. L., and Wolins, N. E. (2016) Isolation of lipid droplets from cells by density gradient centrifugation. *Curr. Protoc. Cell Biol.* **72**, 3.15.11
81. Zhang, S., Wang, Y., Cui, L., Deng, Y., Xu, S., Yu, J., *et al.* (2016) Morphologically and functionally distinct lipid droplet subpopulations. *Sci. Rep.* **6**, 29539
82. Rundén-Pran, E., Mariussen, E., El Yamani, N., Elje, E., Longhin, E. M., and Dusinska, M. (2022) The colony forming efficiency assay for toxicity testing of nanomaterials-Modifications for higher-throughput. *Front. Toxicol.* **4**, 983316